New Directions in
Linear Acoustics and Vibration

Quantum Chaos, Random Matrix Theory & Complexity

Edited by
Richard Weaver

Matthew Wright

11

Mesoscopic seismic waves

Michel Campillo

Laboratoire de Géophysique Interne et Tectonophysique
Observatoire de Grenoble, Université Joseph Fourier and CNRS
France

Ludovic Margerin

Centre Européen de Recherche et d'Enseignement de Géosciences de l'Environnement
Université Paul Cézanne and CNRS
France

This chapter presents recent developments of multiple-scattering and mesoscopic concepts in seismology. After a brief review of classical elastic wave propagation in the Earth, we focus on the scattered waves which form the tail or coda of the signal. The stabilization of vertical to horizontal kinetic energy ratios in the coda is illustrated with data from small crustal earthquakes recorded at a temporary network in California. Using *a priori* geological data, we show that the measurements agree very well with the equipartition principle applied to a layered elastic medium. This confirms that the formation of the coda results from the multiple scattering of elastic waves by Earth's heterogeneities. The concepts of equipartition, diffusion, and energy stabilization are carefully discussed and distinguished with the aid of numerical Monte-Carlo simulations. We underline that energy stabilization occurs much earlier than equipartition, because the latter concept asks for an isotropic energy flux distribution. Having established the importance of multiple scattering in the Earth we explore the role of interference in random seismic wavefields. A brief review of recent experimental and theoretical works on the weak localization of seismic waves is presented. We further explore mesoscopic concepts by demonstrating the close relations between long-time correlation of random seismic waves and the Green's function. Using data from a permanent seismic network in the Alps, we give strong experimental evidence that the correlation of seismic noise contains not only ballistic but also multiply-scattered seismic waves. The power of Green's function reconstruction from random signals is illustrated with applications to seismic tomography and passive monitoring of volcanic activity.

11.1 Introduction: seismic waves and data

Our present knowledge of Earth's dynamics, including plate tectonics, mantle convection, the origin of the magnetic field, etc. is based on the progress of seismological models of the inner structure. Piecewise homogeneous reference Earth models

have been a fundamental step forward in the understanding of the deep interior processes. It has been recognized that those smooth models cannot account for some major observations. One of them is the strong apparent attenuation of ballistic waves, another is its counterpart, the long duration of seismograms with energy arrivals at times that greatly exceed the travel times of the direct waves (see Figure 11.1). This leads to consider the scattering of seismic waves by the inhomogeneity of the material, an inhomogeneity that is widely attested by geological surface observations. In recent years, the attention of seismologists has turned to multiple scattering of elastic waves in the Earth, with a renewal of the investigation of the physics of seismic wave propagation in complex media and of possible mesoscopic effects.

The analysis of the records of ground motion at the surface of the Earth has allowed imaging of the interior of the planet at different scales and quantifying earthquakes. The interpretation of seismograms is made in the framework of the classical theory of elastodynamics. Seismic data consist of time series of the 3D motions recorded at the surface of the Earth. Seismic signals currently cover a frequency band between 0.01 and 10 Hz. Nowadays, most of the recording stations are operated continuously. The sources in most cases produce pulses which are very short with respect to the travel times of the waves. This is not the case with large earthquakes, but that is an issue out of the scope of the present paper. Ballistic waves are usually clearly identified. Their travel times, and often amplitudes, can be described in the framework of the classical ray theory and used for imaging purposes. Whatever imaging technique -body wave tomography or surface wave tomography-, this approach leads to the determination of the local properties of an effective medium (seismic speeds) that can be related to a particular constituent or geological unit. Nevertheless, the ballistic arrivals represent only a small part of the records (see Figure 11.1) and it was realized early that smooth velocity models cannot account for some of the characteristics of seismic signals. The numerous arrivals following the ballistic waves are interpreted as resulting from the scattering in an heterogeneous Earth. These late arrivals are called the seismic coda. For long lapse times, it is characterized by a smooth, exponential-like decay of the energy. It appears that scattering is strong at short periods and tends to be almost negligible for period larger than 30 s. The long coda of short period (around 1 s) seismograms is the most spectacular and direct expression of multiple scattering in the Earth (Figure 11.1).

When considering wave propagation, the solid Earth can be considered as an elastic body. The reader can find a detailed treatment of elasticity in the seismological context in Aki & Richards (2002) for instance. A sample seismogram is shown in Figure 11.2, where three ballistic arrivals can be identified. In an isotropic medium two types of propagating waves exist simultaneously. First mode is the P
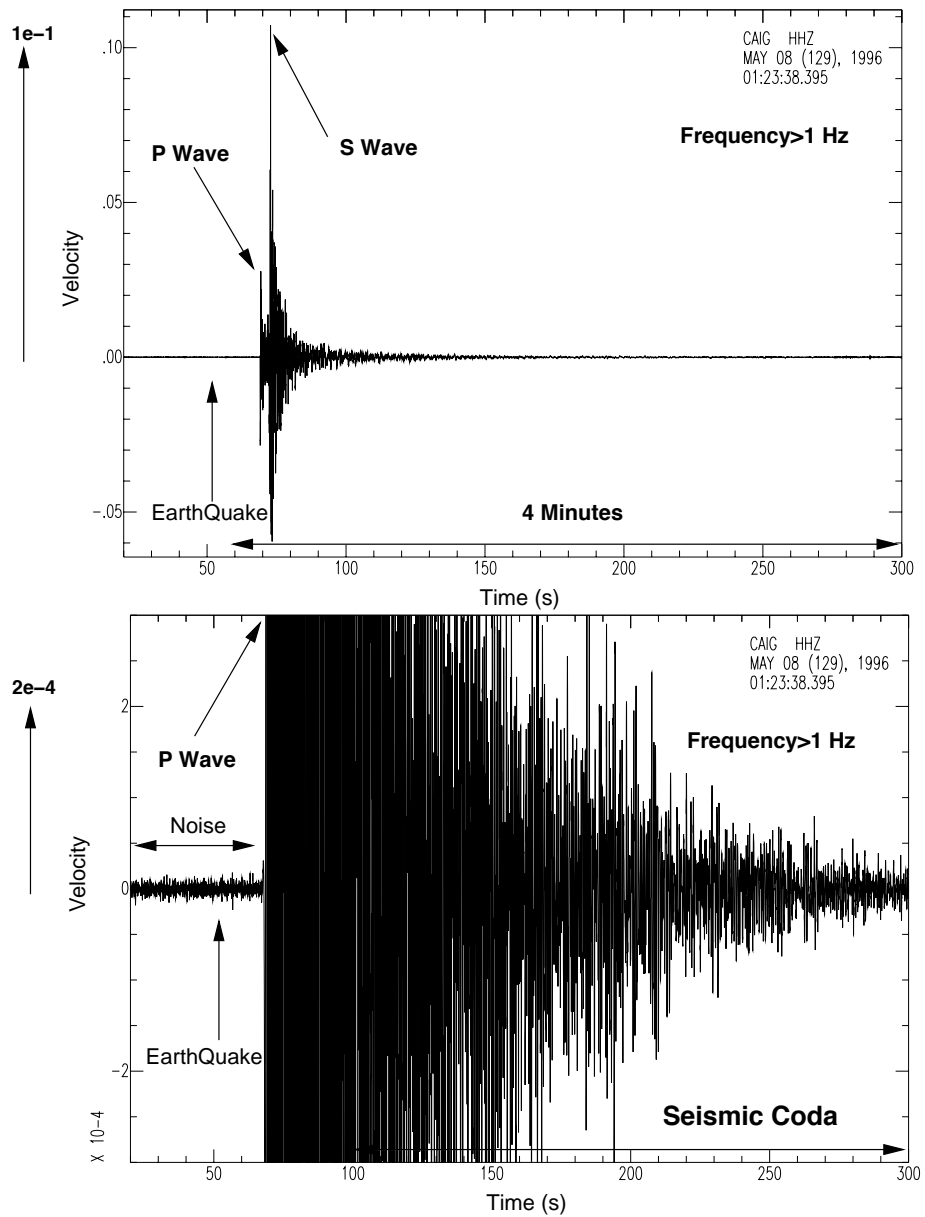
Fig. 11.1. Example of crustal seismogram records. Top: the full range of data is shown. The most prominent arrivals are the ballistic P and S waves. Bottom: the vertical scale has been magnified by a factor 500. The late arrivals form the seismic coda.

wave, a longitudinal wave associated with velocity $\alpha = \sqrt{(\lambda + 2\mu)/\rho}$ where λ and μ denote the two Lamé coefficients and ρ is the medium density. A second

type of wave is the transversely polarized S wave with velocity $\beta = \sqrt{\mu/\rho}$. In the solid materials of the Earth, we often observe that $\alpha \approx \sqrt{3}\beta$. These two modes are coupled and cross converted at each reflection, transmission or scattering. Because of the general trend of increase of velocity with depth, these waves can be trapped in upper layers and give rise to modes of guided waves. A specific coupling between P and S waves is associated with the Rayleigh surface wave. This is the dominant arrival of a broadband seismogram for moderate to large shallow earthquakes as illustrated in Figure 11.2. This perturbation propagates at the surface of an elastic body, even in the case of a homogeneous half-space. It is a combination of inhomogeneous P and S waves (with exponential decay of amplitude with depth) that complies with the zero-stress condition at the surface. It is a specificity of elastodynamics.
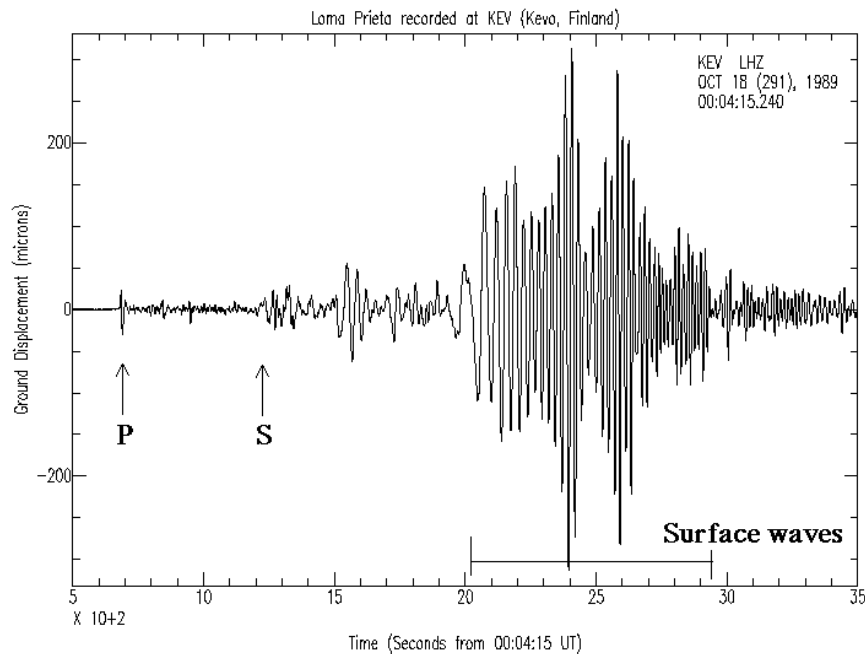

Fig. 11.2. Broadband record of the Loma Prieta Earthquake recorded at the Global Seismic Network station KEV in Finland. The three dominant seismic wave types are shown: Longitudinal or P wave, Transverse or S wave and Rayleigh surface waves. More examples are available at: http://www.quaketrackers.org.nz.

The long duration of seismic signals for local earthquakes recorded in a frequency range between 0.1 and 10 Hz is a clear evidence of scattering in the Earth. This duration greatly exceeds the travel time of direct paths, by a factor 100 in some examples. These late, apparently incoherent arrivals build up the seismic

coda. In Figure 11.1, a typical crustal seismogram illustrates the very large duration of the coda compared to the travel time of ballistic waves. It is also interesting to consider the very large dynamics of seismic records. The coda waves are hardly visible when the full range of the data is shown. Aki & Chouet (1975) showed that the decay with time of the coda envelope is a regional characteristic, independent of the precise location of the station or of the earthquake, or of the earthquake magnitude. According to Rautian & Khalturin (1978), this stationarity of the decay is observed for lapse times larger than twice the travel time of direct shear waves. This rule of thumb has been widely used in coda studies, but it cannot be applied to the case where the source-receiver distance is smaller than the characteristic scale of the scattering process, i.e. the mean free path. The pertinent time scale in coda analysis is the mean free time, i.e. the ratio between the mean free path and the typical wave velocity.

It is difficult to assess the nature of coda waves and their regime of propagation. By using small aperture array of seismometers, it is possible to estimate the distribution of energy on a set of incoming plane waves. While the first arrivals are concentrated in particular directions, the coda is produced by waves arriving from various azimuths and incidence angles, resulting in a speckle pattern which fluctuates with lapse time. This indicates that these waves are produced by scattering on inhomogeneities distributed in the Earth. Whether single scattering, multiple scattering or diffusion should be used to model coda waves has been debated by seismologists since the Aki and Chouet's paper of 1975.

11.2 Equipartition of Seismic Waves

It is difficult to assess the regime of propagation of the waves in a medium with absorption. With elastic waves we can rely on the concept of equipartition that leads eventually to a measurable marker of the diffusive regime, namely the ratio of P to S wave energies (Weaver 1982, Ryzhik et al. 1996). In the seismological context, the predominance of S waves in the coda was discussed in Aki (1992). He showed that the scattering from P to S is much stronger than from S to P. Using an elegant reciprocity argument, he established the following relation between the scattering coefficients:

$$\frac{g_{PS}}{g_{SP}} = \frac{\alpha^4}{\beta^4} \tag{11.1}$$

where α and β are the velocity of P and S waves, respectively. We therefore expect a predominance of S waves in the coda. Dainty & Toksöz (1990) applied array analysis to NORSAR data to show that the coda is dominated by waves with apparent velocities less than 4 km/sec, that is, by S waves.
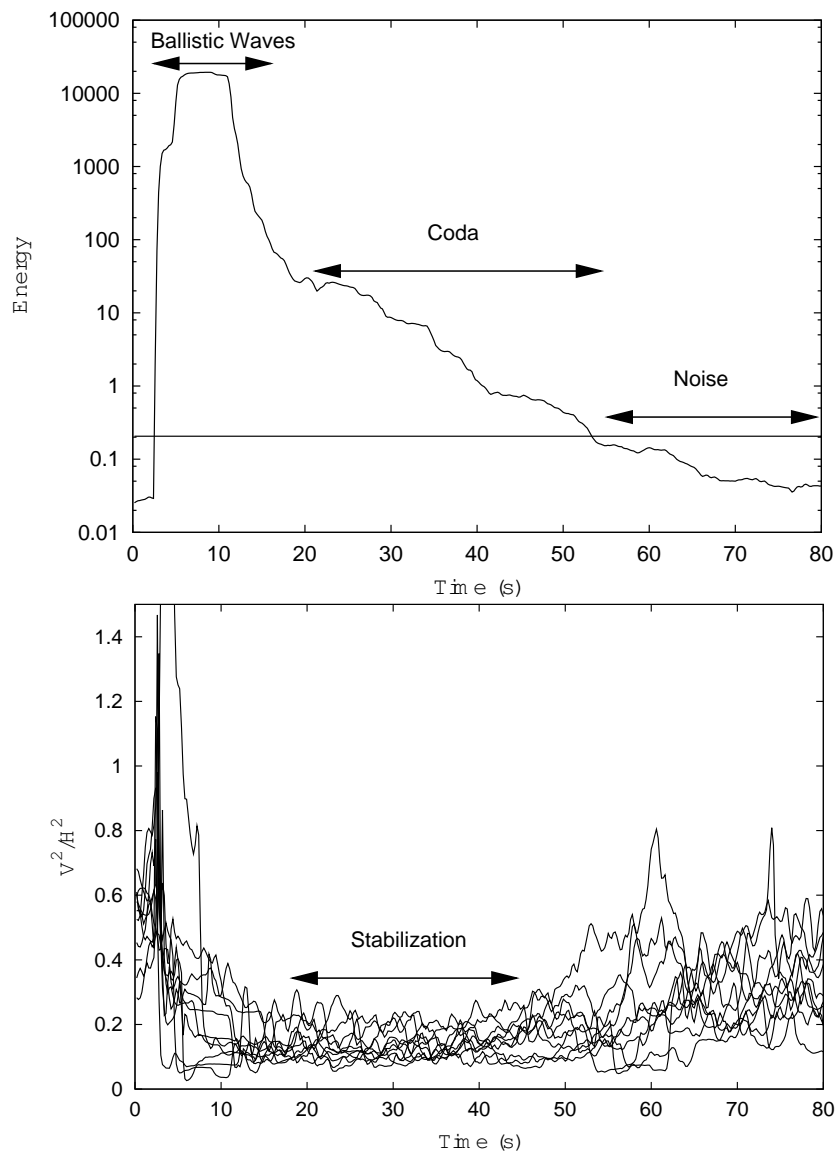
Fig. 11.3. Stabilization of energy ratios in the seismic coda of small earthquakes recorded in California. Top: typical seismogram energy envelope. The horizontal line gives the upper bound for the noise level. Bottom: stabilization of the vertical to horizontal kinetic energy ratio in the coda. Notice the large fluctuations of the energy ratio in direct waves and in the noise.

More generally, in the diffusive regime that emerges after several scatterings, the wavefield is expected to consist of contributions of all possible modes of propaga-

tion. For example in a full space, modes of propagation are pure P and S plane waves. In this case equipartition means that the wave field consists of waves propagating in all directions, with all possible polarizations and equal weights on average. This implies that the relative contribution of P and S waves to the local energy tends to a constant ratio while the energy density itself continuously decays due to the spatial expansion and the anelastic dissipation. A simple mode counting argument allows to compute the ratio of P to S energy at equipartition in a full space (Weaver 1982, Ryzhik et al. 1996):

$$\frac{E_S}{E_P} = 2\frac{\alpha^3}{\beta^3} \tag{11.2}$$

In the case of Poisson solid ($\alpha/\beta = \sqrt{3}$), the full space energy ratio equals approximately 10.4. When there is preferential absorption of one of the modes (P or S), a different stabilization of the energy ratio occurs in the multiple scattering regime (Margerin, van Tiggelen & Campillo 2001). The effect of absorption is to shift the ratio in favor of the mode that is less absorbed. With realistic values of dissipation in rocks, this effect is not expected to strongly affect the observations.

It is useful to further clarify the concept of equipartition and the definition of the underlying set of modes. The set of modes we consider is the one of a reference model on which the disorder is added. The disorder is assumed to be large enough to provoke the coupling between the modes but not to change drastically the structure of the spectrum and eigenfunctions. In other words, the modes we consider are not formally the ones of the actual Earth with all its complexity, but the ones of a fictitious model close enough to essentially share the same spectrum, i.e. essentially the same propagation properties. For a first order computation of the energy ratio, it could be a simple stratified model. Furthermore, we deal here with "local" propagating modes of the lithosphere, that is fundamental and higher-modes surface waves, and body waves leaking into the mantle. It is important to notice that equipartition is expected in the phase space so that it does not mean that the local distribution of energy is the same everywhere in the real space. Locally the ratio is governed by the eigenfunctions of the modes. For example, in the equipartition regime, the contribution of surface waves at the free surface will be larger than at depth due to the decay of the fundamental mode eigenfunction (see Hennino et al. 2001).

Energy stabilization in the seismic coda is illustrated in Figure 11.3. Margerin et al. (2008) have analyzed the vertical to horizontal kinetic energy ratio for ten small earthquakes recorded at a temporary seismic network in Pinyon Flats, California. For a diffuse elastic wavefield in an unbounded medium, this ratio would simply equal 1/2. In the vicinity of a free surface, the Rayleigh wave slightly modifies the theoretical ratio to a value close to 0.56, in excellent agreement with results
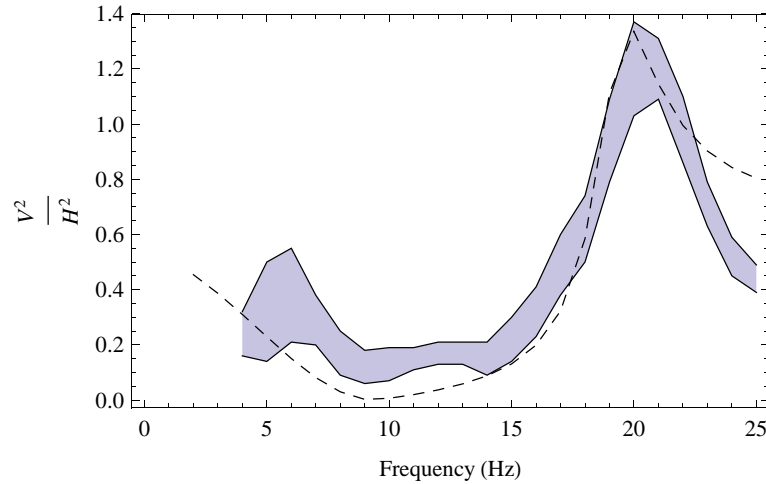
Fig. 11.4. Frequency dependent vertical to horizontal kinetic energy ratio measured at Pinyon Flats (California). The grey area delimits the measurements with uncertainties. The dashed line is the theoretical equipartition prediction from a detailed seismological model of the site.

of Hennino et al. (2001). In Figure 11.3, we remark that the vertical to horizontal kinetic energy ratio in the coda is independent of earthquake location or mechanism in the coda window, whereas this ratio shows large and rapid fluctuations in the noise and in the direct arrivals. In the example shown in figure 11.3, the central frequency of the signal is around 8 Hz and the stabilization ratio lies between 0.1 and 0.2, which is 3 to 4 times smaller than the value reported by Hennino et al. (2001). To understand the difference between this measurement and previous theoretical results obtained for a homogeneous half-space, we have analyzed the frequency dependence of the kinetic energy ratio in the coda in the 5–25 Hz frequency band. The lower frequency is imposed by the sensor sensitivity while the choice of upper bound is dictated by the quality of the signal to noise ratio. The results are shown in Figure 11.4, where a strong frequency dependence is observed. In the 5–10 Hz frequency band, the vertical to horizontal kinetic energy ratio is lower than expected (0.2 instead of 0.56) and shows a sharp peak above 1 around 18 Hz. Since the network was installed on a weathered granite zone, one may expect large differences between the true velocity profile and a simple homogeneous half-space model. Fortunately, (Fletcher et al. 1990) have carefully studied the velocity structure under the array. Using borehole measurements they provided a

detailed model of the subsurface at Pinyon Flats. Applying the equipartition principle to the complete set of modes of a layered elastic half-space including surface and body waves, we were able to calculate the vertical to horizontal kinetic energy ratio for a realistic velocity model at Pinyon Flats. As shown in Figure 11.4, the agreement between observation and theory is satisfactory. This confirms the validity of the equipartition principle and also demonstrates that the coda energy partition contains information on the local geological structure.

What is the significance of the stabilization of energy ratios with respect to the validity of the diffusion approximation and the equipartition itself? Is there an unambiguous relation between stabilization of energy ratio and equipartition? To answer these questions, Figure 11.5 shows numerical solutions of the elastic radiative transfer equation computed with the Monte Carlo approach of Margerin et al. (2000) compared with solutions of the diffusion equation (Paul et al. 2005). The calculations are performed for monodisperse spherical inclusions, with slightly different (5%) density and velocities with respect to a homogeneous matrix. The elastic and scattering properties are representative of Earth's crust: the shear velocity is of the order of 4 km/s, the ratio between P and S velocities equals $\sqrt{3}$, and the ratio between the size of the scatterers and the shear wavelength approximately equals 1. In this regime, scattering occurs preferentially in the forward direction for both P and S waves. Note that because of the elastic isotropy of the medium, mode conversions (P to S and S to P) do not occur in the exact forward and backward directions. The source is assumed to release shear waves isotropically, which is a rough but reasonable approximation for earthquakes. The source station distance and the shear mean free path approximately equal 100 km and 30 km, respectively. The value of the mean free path is representative of the crust for short period waves (frequency > 1 Hz) in tectonically active regions. The numerical simulations indicate that the stabilization of the ratio between P and S energies occurs when the total energy is well approximated by the solution of the diffusion equation (Figure 11.5 upper panels). On the contrary, when considering the angular dependence of the energy flow (Figure 11.5 lower panel), it is clear that the stabilization occurs very early in the evolution of the wavefield toward isotropy. At a time when the stabilization is reached (60s in Figure 11.5), the anisotropy of the field remains strong with a ratio larger than 4 between energies propagating in the forward and backward directions. The diffusion solution itself includes a flow of energy from the source, and therefore an anisotropy of the field. Figure 11.5 also indicates that, when using the diffusion approximation, the anisotropy is underestimated with respect to the radiative transfer equation. We must conclude that the stabilization of S to P energy ratio is a good indication that the field is entering a regime in which the total energy is described by the diffusion equation and therefore will evolve towards equipartition and isotropy. Note that although the computations we just
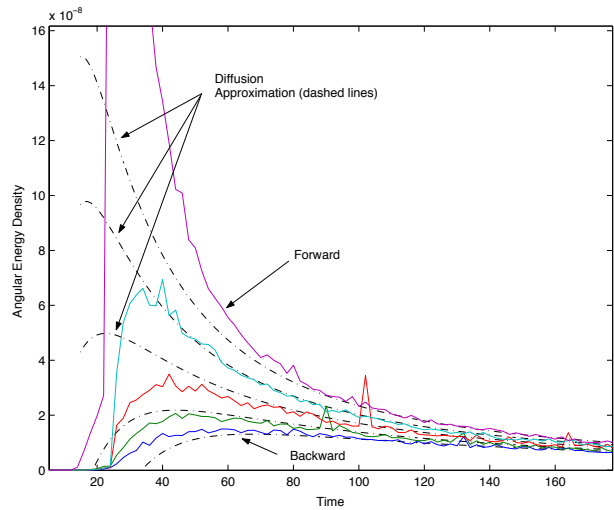
a)
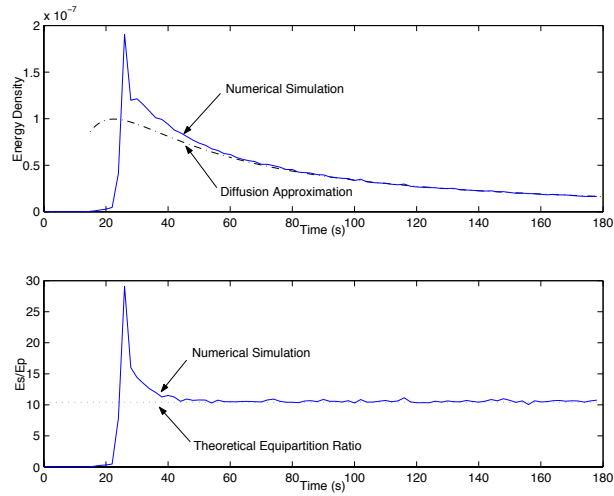
b)

Fig. 11.5. Comparison between numerical (Monte Carlo) solutions of the radiative transfer equation, and analytical solutions of the diffusion equation. Energy density (top), *P* to *S* energy ratio (middle) and angular distribution of elastic energy flux (bottom). The dashed and solid lines show the results of the diffusion approximation and radiative transfer equation respectively. The energy flux decreases monotonically from $\theta = 0$ (forward direction) to $\theta = \pi$ (backward direction), where θ denotes the angle between the propagation direction and the source-observer vector. The results for $\theta = \pi/4$, $\pi/2$ and $3\pi/4$ are also plotted. The source station distance and the shear mean free path equal 100 km and 30 km, respectively. The shear wavespeed is 4 km/s.

presented are performed in a full space, we argue that the conclusion would be much the same in a stratified medium like the Earth.

11.3 Weak localization

Configuration 1
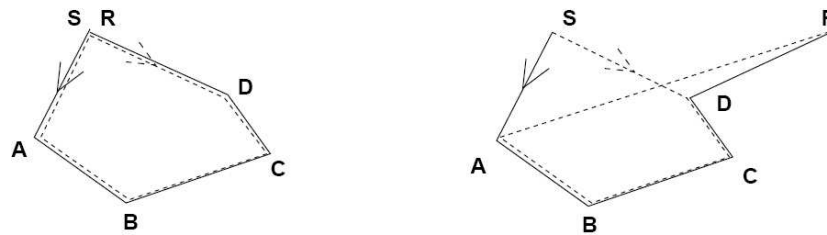
Configuration 2
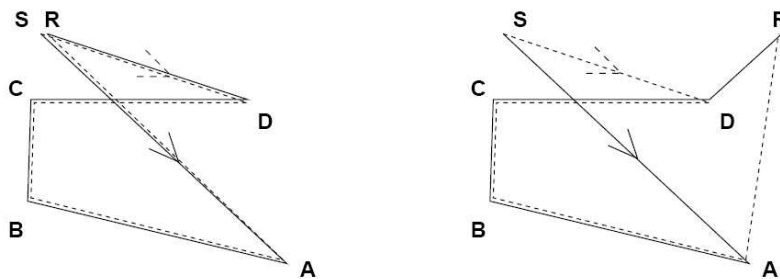

Fig. 11.6. Examples of multiple scattering paths from source S to receiver R. Scattering events are labeled with letters A, B, C, and D. Solid and dashed lines represent direct and reciprocal paths respectively. The two configurations differ by the position of the scattering events. On the left: source and receiver coincide. On the right, source and receiver are typically a few wavelengths apart.

As shown in the previous section, the propagation of multiply-scattered waves is often described by considering the transport of the energy. The energy transport approach has been developed by astrophysicists at the beginning of the twentieth century and has given birth to the theory of radiative transfer (Chandrasekhar 1960, Apresyan & Kravstov 1996). Phenomenologically, the transfer equation for acoustic, electromagnetic and elastic waves can be derived from a detailed local balance of energy that neglects the possible interference between wave packets. This important assumption is justified by the fact that the phase of the wave is randomized

by the scattering events. Thus at a given point, the field can be written as a sum of random phasors and on average, intensities can be added, rather than amplitudes.

The reasoning above misses an important aspect of the wave propagation in multiply-scattering media that is closely related to the reciprocity principle. Let us consider a simple but more detailed argument, where the role of reciprocal scattering paths is emphasized. We represent a scalar partial wave as a complex number $\psi = A e^{i\phi}$, where A and ϕ are real numbers denoting the amplitude and phase, respectively. Each partial wave follows an arbitrarily complicated scattering path from source to receiver in the medium. At a given point, the measured field u is a superposition of a large number of partial waves that have propagated along different scattering paths: $u = \sum_j A_j e^{i\phi_j}$, where the A_j and ϕ_j are random and uncorrelated because of the multiple scattering events, and j can be understood as a "label" for the different paths. Typical examples of scattering paths are shown in Figure 11.6.

Let us now pair direct and reciprocal scattering paths to obtain: $u = \sum_{j'} (\psi_{j'}^d + \psi_{j'}^r)$, where the ψ denote the complex partial waves, the superscripts d and r stand for "direct" and "reciprocal", and a new label j' has been introduced to emphasize the new representation of the field. The intensity I is proportional to $|u|^2$ and reads

$$I = \sum_{j',k'} (\psi_{j'}^d + \psi_{j'}^r)\overline{(\psi_{k'}^d + \psi_{k'}^r)}, \tag{11.3}$$

where the overbar denotes complex conjugation. In equation (11.3), it is reasonable to assume that the waves visiting *different* scatterers will have random phase differences and after averaging over scatterer positions will have no contribution. Thus, we can restrict the summation to the case $j' = k'$ to obtain

$$I = \sum_{j'} \left| \psi_{j'}^d \right|^2 + \left| \psi_{j'}^r \right|^2 + \sum_{j'} (\psi_{j'}^d \overline{\psi_{j'}^r} + \overline{\psi_{j'}^d} \psi_{j'}^r). \tag{11.4}$$

The first term on the right-hand side of equation (11.4) represents the usual incoherent contribution to the measured intensity, which can be calculated with radiative transfer theory. The second term can be interpreted as the *interference* between the direct and reciprocal paths in the scattering medium. In a reciprocal medium, the amplitude and phase of the direct and reciprocal wave paths are exactly the same, i.e $A_j^d = A_j^r$ and $\phi_j^d = \phi_j^r$, provided that source and receiver are located at the same place. Therefore the total intensity which includes the interference term, is exactly double of the classical incoherent term. This is the interference term which is at the origin of the coherent backscattering or weak localization effect.

In seismic experiments performed at the surface, weak localization appears as an enhancement of seismic energy in the vicinity of a source for long lapse times. Margerin, Campillo & van Tiggelen (2001) studied the scalar case in the config-
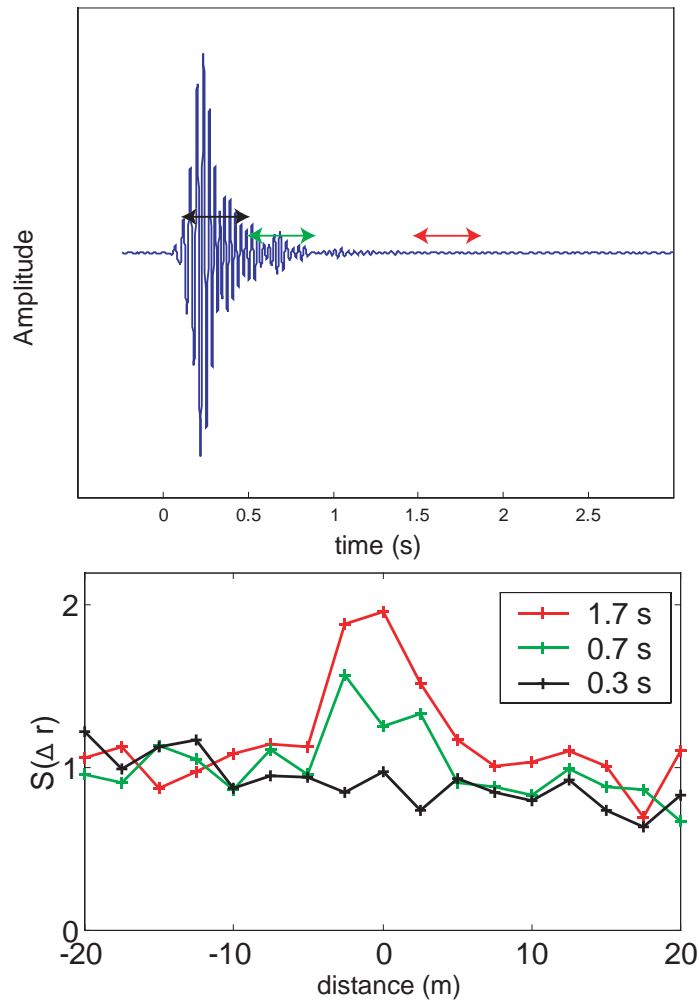
Fig. 11.7. Emergence of weak localization. The upper panel shows an example
of signal produced by a hammer strike. The normalized average energy in the
different time windows is plotted as a function of the distance from the source
(lower panel). Note the absence of enhancement spot for the early coda and the
progressive onset of the weak localization.

uration of a seismic experiment. Note that special care must be given to rules of
reciprocity with polarized waves. The elastic case was treated by van Tiggelen
et al. (2001). A field experiment was performed in a volcanic environment us-
ing a sledge hammer as a source recorded along a profile (Larose, Margerin, van
Tiggelen & Campillo 2004). The energy of the signal is computed in different time
windows of 0.4 s duration. In each window, the energy is normalized by the max-

imum over the array, and then averaged over 12 different configurations. Figure 11.7 shows the average energy enhancement along the profile measured at different lapse times after the passing of the direct waves. As expected from the theory the enhancement shows up progressively for the longer lapse times.

This simple experiment shows a non-intuitive mesoscopic effect that demonstrates that the phase cannot be neglected for seismic waves in the multiply reflected regime. The characteristic time for the onset of the enhancement spot (approximately 0.7 s in the case of Figure 11.7) is the scattering mean-free time, which is a measurement of the heterogeneity of the medium. This type of experiment is a way to measure the mean free time independently of dissipation.

11.4 Field correlations of seismic waves and Green function

Weak localization is an illustration that in complex, apparently random fields, the wave phases are preserved. In the following, we show that the Green function between two points can be retrieved from observations of random fields, in absence of a deterministic source at one of the points. Let us recall a mathematical result that is demonstrated in Colin de Verdière (2006). The wave equation in an arbitrarily heterogeneous medium can be written as:

$$\frac{\partial^2 u}{\partial t^2} + 2a\frac{\partial u}{\partial t} - c^2(\mathbf{r})\Delta u = f \tag{11.5}$$

The attenuation is described by the parameter $a > 0$, $f(t, \mathbf{r})$ is the source field, and $u(t, \mathbf{r})$ denotes a scalar field. When assuming that the source term $f(\mathbf{r}, t)$ has the properties of a white noise, it can be demonstrated that the correlation C between the fields at A and B verifies:

$$\frac{\mathrm{d}}{\mathrm{d}\tau}C(\tau, \mathbf{r}_A, \mathbf{r}_B) = \frac{-\sigma^2}{4a}\big(G_a(\tau, \mathbf{r}_A, \mathbf{r}_B) - G_a(-\tau, \mathbf{r}_A, \mathbf{r}_B)\big). \tag{11.6}$$

In this expression τ is the correlation time, σ is the variance of the source distribution and G_a is the *exact* Green function of the medium. Equation (11.6) can be extended to the case of elastic waves in an arbitrary inhomogeneous medium and generalizes the results of Lobkis & Weaver (2001) for a finite body and Roux et al. (2005) for an infinite medium. Equation (11.6) is reminiscent of the fluctuation-dissipation theorem and has been verified for various kinds of waves in very different frequency bands. (Weaver & Lobkis 2001) showed experimentally that the cross-correlation of the thermal noise recorded at two piezoelectric sensors at the surface of an aluminum sample leads to the complete Green's function between these two points. Local helioseismology (e.g. Duvall et al. 1993, Gizon & Birch 2004, Gizon & Birch 2005) uses cross-correlation of dopplergrams to reconstruct acoustic body waves propagating in the Sun.

The direct application of expression (11.6) to seismology seems rather limited since evenly distributed random sources do not exist in the Earth. For instance, earthquakes occur on localized fault systems. Thanks to modern seismological instrumentation, a huge quantity of continuous records are now available. In absence of earthquakes, a permanent motion of the ground is recorded. We refer to it as "ambient noise". For periods larger than 1 s, this background "noise" results from the mechanical coupling between the solid Earth and its fluid envelopes. The oceanic wave activity is a prominent cause for periods between 1 and 40 seconds. Numerous observations suggest that the sources of seismic noise in the 5-40s period band change position with time, exhibiting a clear seasonality (e.g. Stehly et al. 2006). This time-varying distribution of sources makes it possible to reconstruct efficiently the surface wave part of the Green function by correlating long time series of noise (Shapiro & Campillo 2004). Interestingly, the long range correlations of coda waves were also proved to contain the surface wave part of the Green function (Campillo & Paul 2003, Paul et al. 2005). In this last case, it is the multiple-scattering process which generates the random distribution of sources. The reconstructed Rayleigh waves can in turn be used for tomographic studies as shown by e.g. Shapiro et al. (2005). We refer to Campillo (2006), Larose, Margerin, Derode, van Tiggelen, Campillo, M.Shapiro, Paul, Stehly & Tanter (2006) and Gouédard et al. (2008) for further details on the correlation properties of seismic noise and coda waves.

Since 2005, the use of noise correlation for seismic tomography is a rapidly growing field. There are nevertheless several issues which must be clarified. The reconstruction of the Green function is not perfect in practice, even when the correlation is computed for very long time series of noise (up to several years). The fluctuations of the correlation around the Green function remain significant. It is therefore difficult to identify other arrivals than the predominant surface wave. The convergence towards the Green function, i.e. the ratio between the Green function amplitude and the residual fluctuations, is expected to evolve as the square root of the amount of data used in the cross-correlation (Larose, Margerin, van Tiggelen & Campillo 2004, Snieder 2004, Sabra, Roux & Kuperman 2005, Weaver & Lobkis 2005). With actual data, the perfect convergence cannot be achieved. This is caused by some deterministic and permanent structures of the seismic noise that remain after averaging, such as spatially localized sources and temporal correlations of the excitation. How can we demonstrate that waves other than direct surface waves are also present in the correlations, as expected from equation (11.6)? We performed a specific experiment with real data to demonstrate the presence of multiply-scattered waves in the Green function obtained from noise correlation (Stehly et al. 2008). The basic idea is that, if diffuse coda waves are present in the correlations, their correlations should in turn contain the Green function. In

other words the correlation of coda of correlations between two stations A and B—referred to as the C^3 function—contains the direct waves between stations A and B. To illustrate this idea, we used data from European stations located in and around the Alps. Let us consider two stations EMV and GIMEL whose location is shown in Figure 11.8. We compute noise correlations between the station EMV (resp. GIMEL) and all other stations of the network located at regional distances (see Figure 11.8). Formula 11.6 indicate that these correlations must contain direct and coda waves albeit with various signal to noise ratios. We consider these correlation functions as equivalents of seismograms produced by sources acting at regional distances and recorded at EMV and GIMEL. We select time windows corresponding to coda waves and compute the average correlation between the virtual seismograms at EMV and GIMEL. Just like for earthquake data (Campillo & Paul 2003, Paul et al. 2005), after averaging over the 100 stations of the network, the C^3 function clearly exhibits the direct arrivals of the Green function (see Figure 11.8). It is therefore possible to extract clear direct arrivals from late time windows of the correlation function which are apparently dominated by random fluctuations. This experimental result shows that noise correlations actually contain multiply scattered waves.

11.5 Tomography and temporal changes from seismic noise

Even though only surface waves have been reconstructed from noise so far, it is a valuable result because dispersive surface waves are widely used for imaging crustal or lithospheric shear velocity structures. Shapiro et al. (2005) were the first to use seismic noise to map the distribution of Rayleigh wave group velocities across California. After this first successful application, the noise-based surface wave tomography has been rapidly emerging as a powerful method for imaging the Earth's crust and uppermost mantle at local and regional scales. Numerous applications can be cited: Sabra, Gerstoft, Roux, Kuperman & Fehler (2005) and Moschetti et al. (2007) in Western United States; Yang et al. (2007) and Villasenor et al. (2007) in Europe; Lin et al. (2007) in New Zealand; Kang & Shin (2006) in Korea; Yao et al. (2006) in China; Nishida et al. (2008) in Japan. In recent work Stehly et al. (2008b) applied the noise-based Rayleigh-wave tomography to image the structure beneath the Alpine region with the European Seismic network. They used the correlation of the seismic ambient noise to study the lithosphere. Cross correlation of one year of noise recorded at 150 broadband stations yields more than 3000 Rayleigh group velocity measurements. These measurements are used to construct Rayleigh group velocity maps of the Alpine region and the surrounding areas in the period band between 5 and 80s. The local dispersion curves are then inverted to obtain depth dependent shear wave velocity. The results of
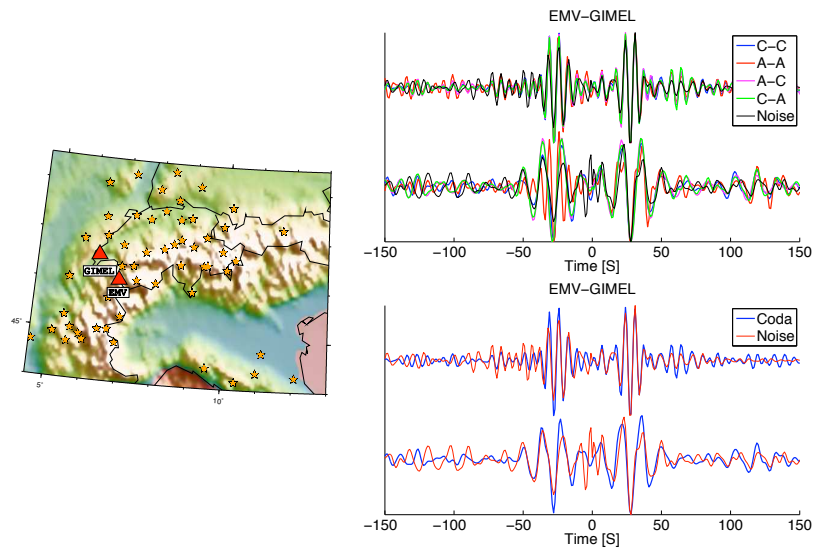
Fig. 11.8. Left: location map of the permanent seismic network in the Alps. Right, upper panel: Green's function between stations EMV and GIMEL (shown left) reconstructed by correlating one year of noise records (black) and by correlating coda waves reconstructed by noise correlations (C3, in blue). We show with different colors the C3 functions, where the coda was selected on the positive noise correlation time, negative time or a mix of the two. Right, lower panel: noise correlation function between EMV and GIMEL (red) and the stack of the 4 (C3) functions. We show the results for two period bands: 5–10s (Top) and 10–20s (Bottom).

this processing are illustrated in Figure 11.9 where the depth of the crust-mantle boundary is presented. The thickening of the crust in the axis of the Alps is well imaged with this passive imaging approach.We also demonstrated that the noise-based imaging can be applied to relatively short period (1-5 s) Rayleigh waves to study internal structure of volcanic edifices with an application to the Piton de la Fournaise volcano on La Réunion island (Brenguier et al., 2007).

The correlation technique can also be used for other applications than tomography. By computing noise cross-correlations between different receiver pairs for consecutive time periods, we let each receiver act as a virtual highly repetitive seismic source, allowing us to detect changes in the Earth mechanical properties. We already made a series of applications (Stehly et al. 2007, Brenguier et al. 2008). In Stehly et al. (2007) we selected a series of records obtained during long periods (more than 10 years). This analysis allowed us to determine the duration of averaging required to obtain stable measurements. This point is strongly linked to the question of the origin of the seismic noise. Stehly et al. (2007) proposed a method
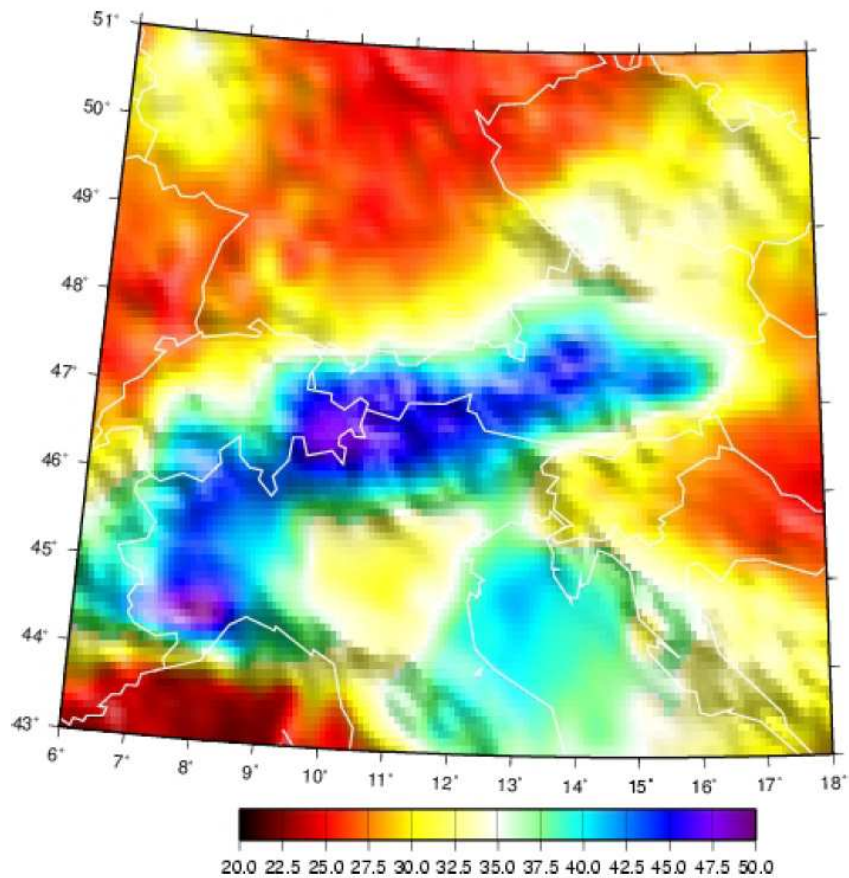
Fig. 11.9. View of the Moho beneath the alps. This image was obtained from seismic noise only. Records from broad band European network were cross correlated to construct the Green function between each pair of stations and a 3D tomography was performed based on local Rayleigh wave dispersion properties (modified from Stehly et al. (2008b))

to correct for instrumental errors which is based on the property of time symmetry of the wave equation. We then applied the repetitive noise-based measurements to study the Piton de la Fournaise volcano on La Réunion island and demonstrated that the associated reconstructed seismic waves (Green functions) can be used to detect temporal perturbations associated with small velocity changes. The accuracy of the measurements of relative velocity change is better than 0.1% (Brenguier et al. 2008). In particular we observed a new type of precursory phenomenon. The pre-eruptive dilatations of the Piton de la Fournaise volcano provokes a slight decreases of seismic velocity a few days prior to eruptions. Noise based monitoring is precise enough to detect such changes of velocity (Figure 11.10). The measure-

ments reach a high accuracy level because we associate the noise-based reconstruction with a doublet analysis that takes advantage of the presence of scattered waves (Poupinet et al. 1984, Grêt et al. 2005, Sens-Schönfelder & Wegler 2006, Wegler & Sens-Schönfelder 2007). The technique is similar to the Diffuse Wave Spectroscopy used in optics and acoustics (see Snieder & Page (2007) for a review of recent results).
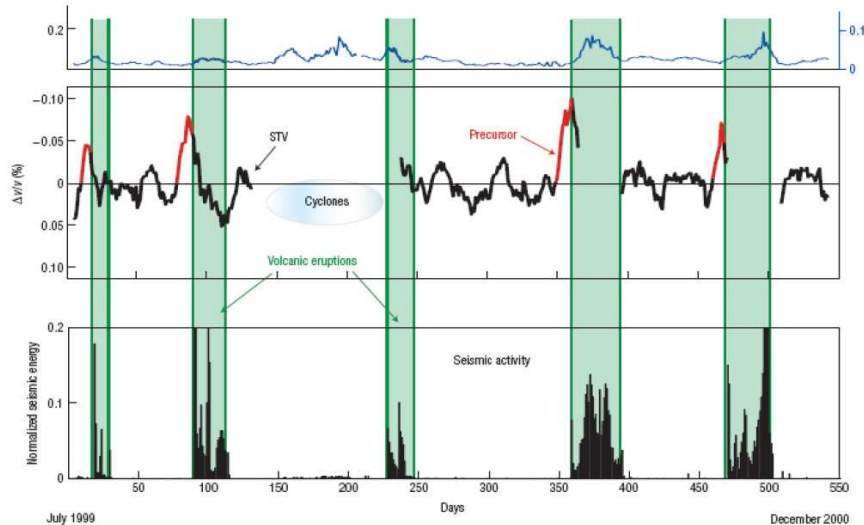

Fig. 11.10. Evolution of relative velocity changes on Piton de la Fournaise over 18 months. Top: The blue error curve represents the uncertainty on the time delay. Measurements with uncertainties higher than 0.04% are excluded from the analysis. Middle: Short term evolution of the velocity computed as relative velocity changes corrected for a long-term component (LTV). Bottom: Daily seismic activity measured by a sensor located near Dolomieu crater.

11.6 Conclusion

We have tried to demonstrate the usefulness of multiple-scattering and mesoscopic concepts in seismology. We have put emphasis on the experimental illustration of the closely related phenomena of equipartition and long-range field correlations. A large number of applications are currently being developed such as seismic tomography with ambient noise. Recently, the possibility to monitor local, small temporal variations in active regions with seismic noise has been demonstrated (Wegler & Sens-Schönfelder 2007, Brenguier et al. 2008), which opens new ways for the investigation of the Earth dynamics. This illustrates the possibility to do mesoscopic physics with signals that are themselves the output of mesoscopic seismic

experiments. Long range correlations (Stehly et al. 2008) and weak localization (Larose, Lobkis & Weaver 2006) have also been observed in the coda of signals resulting from the cross-correlation of ambient or thermal noise. The far-reaching implications of mesoscopic concepts for seismology are still to be further explored.